Quaternary Science Reviews 101 (2014) 77–90

Contents lists available at ScienceDirect

Quaternary Science Reviews

journal homepage: www.elsevier.com/locate/quascirev

Constraints on the late Quaternary glacial history of the Inylchek and Sary-Dzaz valleys from *in situ* cosmogenic ^{10}Be and ^{26}Al, eastern Kyrgyz Tian Shan

Nathaniel Lifton [a, b, *], Casey Beel [a], Clas Hättestrand [c], Christine Kassab [a], Irina Rogozhina [d], Richard Heermance [e], Michael Oskin [f], Douglas Burbank [g], Robin Blomdin [a, c], Natacha Gribenski [c], Marc Caffee [b], Brent M. Goehring [a], Jakob Heyman [c], Mikhail Ivanov [h], Yanan Li [i], Yingkui Li [i], Dmitry Petrakov [h], Ryskul Usubaliev [j], Alexandru T. Codilean [k], Yixin Chen [l], Jon Harbor [a, c], Arjen P. Stroeven [c]

[a] Department of Earth, Atmospheric, and Planetary Sciences, Purdue University, West Lafayette, USA
[b] Department of Physics and Astronomy, and Purdue Rare Isotope Measurement Laboratory (PRIME Lab), Purdue University, West Lafayette, USA
[c] Department of Physical Geography and Quaternary Geology, and Bolin Centre for Climate Research, Stockholm University, Stockholm, Sweden
[d] German Research Centre for Geosciences, Potsdam, Germany
[e] Department of Geological Sciences, California State University, Northridge, USA
[f] Department of Earth and Planetary Sciences, University of California, Davis, USA
[g] Department of Earth Science, University of California, Santa Barbara, USA
[h] Faculty of Geography, Lomonosov Moscow State University, Moscow, Russia
[i] Department of Geography, University of Tennessee, Knoxville, USA
[j] Central Asian Institute of Applied Geosciences, Bishkek, Kyrgyzstan
[k] School of Earth and Environmental Sciences, University of Wollongong, Wollongong, Australia
[l] College of Urban and Environmental Sciences, Peking University, Beijing, China

ARTICLE INFO

Article history:
Received 28 November 2013
Received in revised form
19 June 2014
Accepted 30 June 2014
Available online

Keywords:
Glacial history
Tian Shan
Paleoglaciation
Cosmogenic nuclides

ABSTRACT

Paleoclimatic constraints from regions at the confluence of major climate systems are particularly important in understanding past climate change. Using geomorphic mapping based on remote sensing and field investigations, combined with *in situ* cosmogenic ^{10}Be and ^{26}Al dating of boulders associated with glacial landforms, we investigate the chronology of past glaciation in the Inylchek and Sary-Dzaz valleys in the eastern Kyrgyz Tian Shan, a tectonically active area with some of the highest peaks in the world outside of the Himalayas. Cosmogenic ^{10}Be and ^{26}Al exposure ages of boulders on moraines record up to five glacial advances including: Lateglacial age lateral moraine remnants and meltwater channels in the upper Inylchek Valley; Last Glacial Maximum (LGM, Marine Oxygen Isotope Stage [MIS] 2) moraines in the Sary-Dzaz Valley and in a terminal moraine complex at the west end of the Inylchek Valley, overriding older moraines; an MIS 4 or 5 moraine remnant above the Inylchek terminal moraine complex; and an older high moraine remnant down-valley from the confluence of the Inylchek and Sary-Dzaz valleys. The evidence for glacial extent in this study is consistent with a limited ice expansion hypothesis for Tian Shan glaciation. Published results from the western and central Kyrgyz Tian Shan do not show evidence for significant LGM glacier expansion, which in combination with the results presented here, indicate a spatial variation in glacier records along the Tian Shan. This may reflect either paleoclimatic gradients or the impact of local physiographic conditions on responses to regional climate change, or both.

© 2014 Elsevier Ltd. All rights reserved.

1. Introduction

Testing global climate models requires well-constrained information on past climates for key regions of the world. Particularly important are paleoclimatic constraints from regions at the

* Corresponding author. Department of Earth, Atmospheric, and Planetary Sciences, Purdue University, West Lafayette, USA. Tel.: +1 765 494 0754; fax: +1 765 496 1210.
E-mail address: nlifton@purdue.edu (N. Lifton).

http://dx.doi.org/10.1016/j.quascirev.2014.06.032
0277-3791/© 2014 Elsevier Ltd. All rights reserved.

confluence of major climate systems, because transitional regions can display increased sensitivity to changes in regional patterns of climate (Rupper and Roe, 2008; Rupper et al., 2009). Central Asia is at the confluence of several significant climate systems, including the Mid-latitude Westerlies and the Siberian High pressure system. Temporal variations in these regional atmospheric circulation patterns will likely impact the numerous glacial systems that play a role in establishing the overall hydrology of this area. Understanding the responses of these glaciers in terms of climate change is important as they provide freshwater to numerous local and distant communities (e.g., Sorg et al., 2012).

The Tian Shan is a WSW–ENE trending arc of mountains in Central Asia, stretching ~2500 km from the western boundary of Kyrgyzstan across most of the Xinjiang Uighur Autonomous region in China. Its highest peaks are Jengish Choqusu (in Kyrgyz, also called Tuo Mu Er in Chinese and Pobeda Peak in Russian) at 7439 m above sea level (m a.s.l.) and Khan Tengri at 7010 m a.s.l., both on the border of easternmost Kyrgyzstan, Kazakhstan and China. Although the Tian Shan is an important physical climate barrier in the transition between the climate of western China and that of southern Siberia, its paleoclimate has received insufficient attention, in part because of the challenges of working in this area.

The present climate in the Tian Shan is dominated by the Mid-latitude Westerlies. This range is beyond the northern limit of the influence of contemporary monsoon climate systems (Dolgushin and Osipova, 1989), although Dortch et al. (2013) suggested the possibility that past climatic patterns were different. Most glaciers in the Tian Shan are retreating as a result of climate change (Dyurgerov, 2010), but the rate of glacier recession varies markedly across the range (Narama et al., 2010) with glaciers at its periphery showing the highest mass losses (Aizen et al., 2007; Bolch, 2007; Sorg et al., 2012; Osmonov et al., 2013). A more detailed reconstruction of glaciation in the Tian Shan is essential for understanding the complex impacts of changes in climate patterns, in particular the interaction of the Westerlies, the Siberian High, and monsoons. It seems likely that most scenarios under a warming climate will result in fewer water resources in this area. As such, better management of this water resource (e.g., Koppes et al., 2008; Rupper et al., 2009; Sorg et al., 2012) may be possible with advances in our understanding of the interplay between climate and hydrological resources.

Previous work in the western Tian Shan provides strong evidence for multiple periods of glacial activity (e.g., Dikikh et al., 1991; Koppes et al., 2008; Zech, 2012). Few absolute dates on the glacial landforms that have been mapped are available, and considerable doubt remains about the timing of these glacier expansions when compared to global climate events recorded in other regions. The consensus of most published work is that major glaciations in this region were limited to expansion of isolated glaciers, although Grosswald et al. (1994) and Kuhle (2004) present an alternative hypothesis that includes a large ice sheet up to 2.5 km thick in this area during the Last Glacial Maximum (LGM, Marine Oxygen Isotope Stage [MIS] 2, 14–29 ka, Lisiecki and Raymo, 2005). This wide disparity in reconstructed ice extents indicates a need to carefully re-evaluate key field and chronological evidence used in the alternate models.

To investigate long-term responses of glaciers to past climatic shifts, we have assembled an international team to reconstruct patterns and timing of past glaciation along major transects across Central Asia (e.g., Heyman et al., 2008; Stroeven et al., 2009; Li et al., 2011; Heyman et al., 2011a; Fu et al., 2012, 2013; Stroeven et al., 2013; Heyman, 2014; Li et al., 2014). The focus of this study is the eastern Kyrgyz Tian Shan (Fig. 1). In addition to remote sensing efforts to map out the glacial landforms of the Tian Shan (Fig. 1B) (Stroeven et al., 2013), we have collected rock samples for *in situ* cosmogenic nuclide dating of moraines that delineate the former extents of glaciers draining the Jengish Choqusu and Khan Tengri massifs through the Inylchek and Sary-Dzaz valleys (Figs. 1C and 2).

1.1. Study area

The Tian Shan comprises a series of generally east-northeast trending mountain ranges and intermontane basins in Central Asia, extending from western Kyrgyzstan/Uzbekistan east into China (almost to Mongolia). The range formed in response to the northward propagation of the India–Asia collision that focused deformation along pre-existing east–west oriented zones of crustal weakness between the Tarim Basin to the south and the Kazakh craton to the north (Yin, 2010; Zubovich et al., 2010). These faults typically exhibit oblique or reverse slip (e.g., Tapponnier and Molnar, 1979; Omuralieva et al., 2009). Currently, almost half of this convergence is absorbed along faults in the central Asian interior ranges – about 20 mm/yr across the Tian Shan (Abdrakhmatov et al., 1996; Zubovich et al., 2010). Neogene deformation distributed across the Tian Shan has resulted in some of the world's highest peaks outside the Himalayas, particularly in eastern Kyrgyzstan along the border with China and Kazakhstan.

Large glaciers drain the Jengish Choqusu and Khan Tengri massifs, including the Northern Inylchek and Southern Inylchek glaciers draining into the Inylchek Valley, and the Semyonov and Mushketov glaciers draining into the Sary-Dzaz Valley to its north (Fig. 1C). These glaciers are a major water source for northern Chinese communities, via the Inylchek, Sary-Dzaz, and ultimately the Aksu rivers. Of importance, in this regard, is that seasonal meltwater comes in highly irregular pulses through the Aksu River drainage system because of the seasonal drainage of Merzbacher Lake, an ice-dammed lake that forms annually in the terminal zone of the Inylchek glacier system (e.g., Aizen et al., 1997; Glazirin, 2010; Häusler et al., 2011; Li et al., 2013; Xie et al., 2013). Despite the importance of glaciers as a freshwater resource, the behavior of these glacier systems over glacial–interglacial timescales (Li et al., 2011), including the Holocene (Solomina, 1999), is not well documented.

Much of the Inylchek Valley depression appears to be a consequence of the underlying Atbashi-Inylchek fault, a major left-oblique slip fault that forms the southern boundary of the Sary-Dzaz Range (Fig. 1C). This portion of the Inylchek Valley is linear but transitions to an abrupt southward-trend immediately downslope from the Inylchek settlement (Fig. 2B), perhaps in response to a releasing bend forming what has been mapped as a pull-apart basin (Mikolaichuk et al., 2008). The southern slope of the Sary-Dzaz Range is characterized by a series of moraines, terraces, ridges and channels, spanning ca 800 m in altitude from the present Inylchek Valley bottom (Fig. 2A), yet glaciers within the range are currently restricted to the uppermost sections of the slope (Fig. 1C). In contrast, the northern slope of this range, draining to the Sary-Dzaz Valley, is characterized by less pronounced relief, yet it exhibits significantly more abundant and pronounced glacial features (Fig. 2D). Another major left-oblique slip fault zone, the Nikolaev Line, underlies the Sary-Dzaz Valley and is thought to intersect the Atbashi-Inylchek fault near the eastern sector of this valley (Fig. 1C).

1.2. Previous work

Until recently, modern paleoglaciological research in the eastern Tian Shan in China has been largely restricted to the source area for the Ürümqi River (northern slope of the Tianger Range; Fig. 1B, 43.1°N, 86.5°E); the Glaciological Research Station of the Chinese Academy of Sciences facilitates studies of glacial and Quaternary geology, including recent chronological research (e.g., Yi et al.,

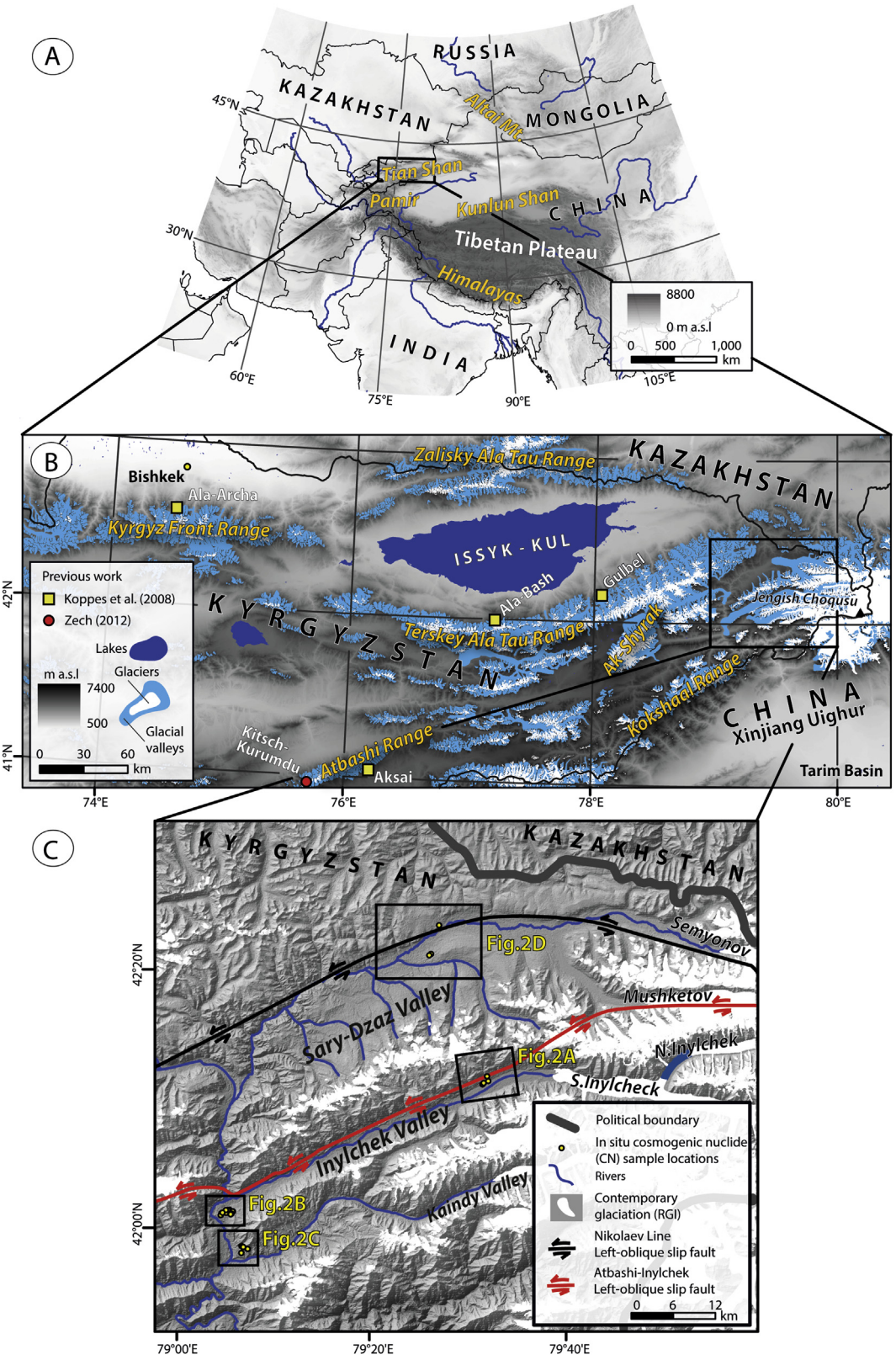

Fig. 1. A – Map of Central Asia showing the location of the Tian Shan and Panel B. B – Aster Global Digital Elevation Model V2 (Aster GDEM2, http://asterweb.jpl.nasa.gov/gdem.asp, developed jointly by the U.S. National Aeronautics and Space Administration and the Japanese Ministry of Economy, Trade, and Industry) of Tian Shan and the distribution of glacial valleys (Stroeven et al., 2013) mapped from a slope model computed from the Shuttle Radar Topographic Mission (SRTM) DEM (http://www2.jpl.nasa.gov/srtm/). Glacier outlines are taken from the Randolph Glacier Inventory (Arendt et al., 2012) (RGI, http://www.glims.org/RGI/) Box denotes outline of Panel C. C – Hillshade model of the Inylchek- and Sary-Dzaz valleys computed from the Aster GDEM2 data. Map shows location of *in situ* cosmogenic nuclide samples, contemporary glaciated areas (RGI), locations of the Atbashi-Inylchek fault and Nikolaev line (Konopelko et al., 2007) and black boxes show locations of detailed maps (Fig. 2A–D).

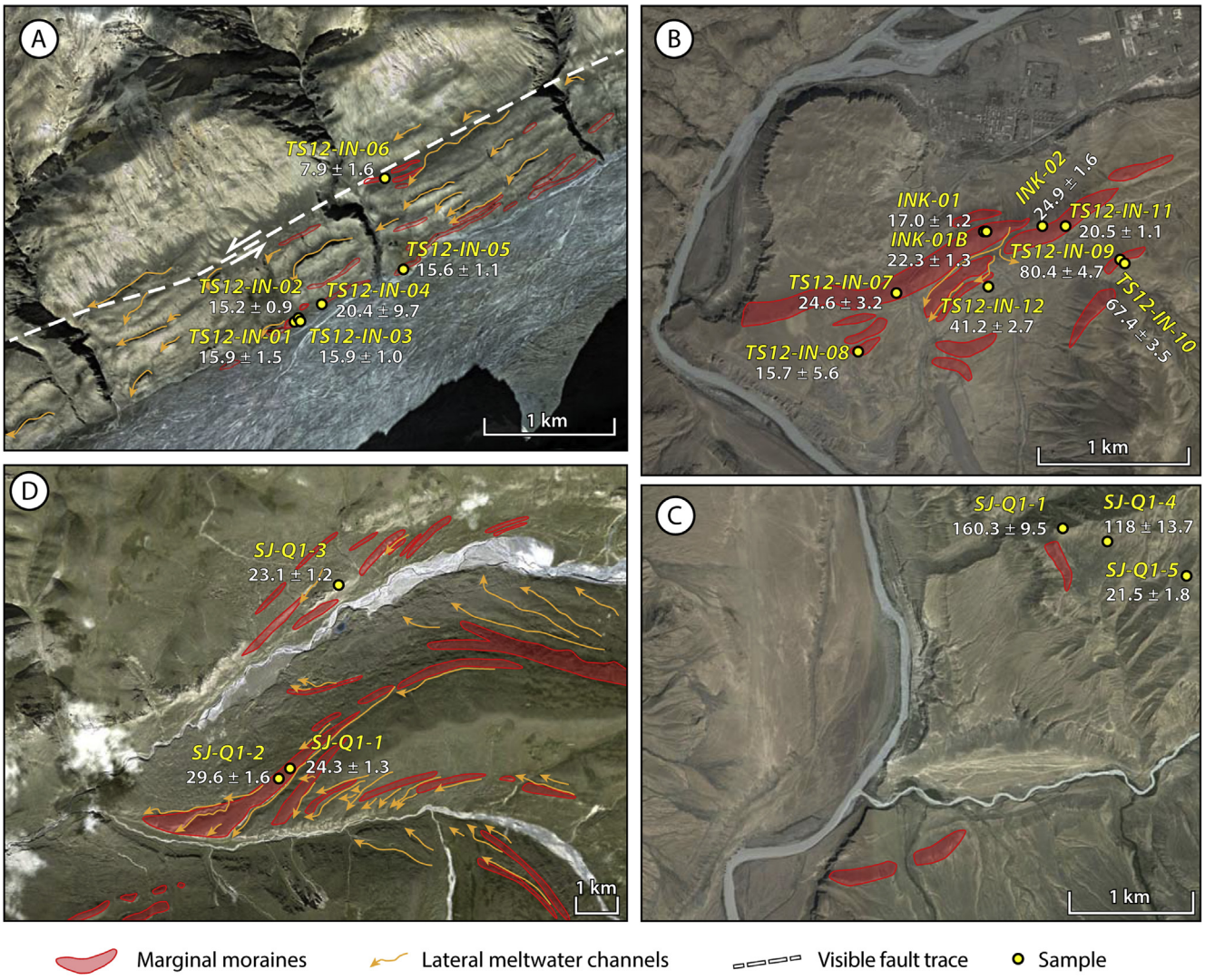

Fig. 2. Glacial geomorphology of the sample areas (see Fig. 1 for location), marked on satellite images (Google Earth, v. 7.1.1.1888, 2013; CORONA satellite imagery, frame DS1112-2201DA037_a, 12/1970: http://eros.usgs.gov/satellite-imagery). *In situ* cosmogenic ^{10}Be ages in white, sample numbers in yellow italics. Panels are numbered clockwise from upper left. A: Upper Inylchek Valley, B: Lower Inylchek Valley, C: Lower Inylchek high moraine remnant, D: North–central Sary-Dzaz Valley. All panels have geographic north to the top.

2002, 2004; Zhou et al., 2002; Zhao et al., 2006; Kong et al., 2009; Li et al., 2011, 2014). These studies document a rich glacial record, but also indicate wide variations in ages derived using different dating techniques, leading to considerable controversy about the timing of events.

The glacial histories of the Tian Shan in Kyrgyzstan, by comparison, have not been studied in as much detail using numerical dating techniques, despite accounts of vast glaciated areas during the LGM noted by Mushketov (1915). Severtsov (1873) provided the first published evidence of the Pleistocene extent of glaciers in the Kyrgyz Tian Shan, and of a glaciological expedition to the heart of the Kyrgyz Tian Shan led by Ignatiev in 1886, who discovered the Inylchek Glacier. Mushketov (1915) concluded that prior glaciations in the Kyrgyz Tian Shan were more restricted in extent than similar events in the Alps and, based on observations by Merzbacher (1905), concluded there were 2–3 Pleistocene glacial stages. Demchenko (1935) suggested that the Northern Inylchek Glacier was a tributary of the Southern Inylchek Glacier during the LGM and that, together, they filled the entire Inylchek Valley. Research organized during the Soviet period (e.g., Aleshinskaya, 1971; Aleshinskaya et al., 1976; Bondarev, 1976; Lebedeva, 1982), in which ages of glacial landforms were assigned on the basis of their inferred correlations with radiocarbon-dated lake and river terraces (Chedia, 1986), concluded that the LGM advance of glaciers in Central Asia happened before 23–25 ka and after 15–18 ka (Nikonov, 1982). Nikonov (1982) further argued that determining the timing of the LGM would be key for future work on the paleogeography of this region.

A summary of much of the Soviet-era research on the extent of LGM glaciation in the Kyrgyz Tian Shan is embodied in a 1:3,000,000 "map of maximum glacier extent during the LGM" in the World Atlas of Snow and Ice Resources (1997). This map shows that the Inylchek Valley was completely filled with a valley glacier during the LGM, which is dated as 17–21 ka – consistent with the conclusions of Nikonov (1982). The only detailed study focusing on the glacial history of the Inylchek valley during the Soviet era was by Dikikh et al. (1991), who assessed the ages of moraines in the lower Inylchek valley using the stratigraphic approach of Chedia (1986). Dikikh et al. (1991) concluded that the age of the so-called Sarlytash (lateral) and Kumbulun (bottom) moraines in the Inylchek and Sary-Dzaz valleys close to the Inylchek settlement was 50–60 ka, which is much older than the ages shown in the World

Atlas of Snow and Ice Resources (1997). In a more regional study, Bondarev (1976) suggested that the maximum ice thickness in the Inylchek Valley during past glaciations was ca 700 m. Kachaganov (2011) noted that the most challenging question in Kyrgyz Tian Shan Quaternary stratigraphy concerns the correlation between river terraces and moraines and suggested that absolute dates for glacial landforms were needed to improve an understanding of the regional glacial history.

In direct contrast to the reconstruction of glacier extents during the LGM from the World Atlas of Snow and Ice Resources (1997), Grosswald et al. (1994) and Kuhle (2004) proposed a very different scenario. Using field mapping, radiocarbon dating, and ice-sheet modeling, they suggested an order of magnitude larger area of glacierization in the Kyrgyz Tian Shan during the LGM, including an ice sheet with ice thicknesses up to 2500 m. This is a controversial model; Owen and Dortch (2014) reviewed the issues surrounding this debate. They argue that Kuhle's (2004, 2011) conclusions are at odds with the bulk of glacial geomorphic evidence, which in turn is constrained by optically stimulated luminescence (OSL) and terrestrial cosmogenic nuclide dating techniques (Owen and Dortch, 2014). More recent systematic mapping of the glacial geomorphology of the Tian Shan by Stroeven et al. (2013), based on the Shuttle Radar Topography Mission digital elevation model (at 90 m resolution), Landsat 7 ETM + satellite imagery (at 30 m resolution), and Google Earth, shows that landforms created by glaciers in the Tian Shan were restricted to mountain areas and their immediate surroundings and are not consistent with a large ice sheet model for LGM glaciation.

Studies using advanced dating methods to constrain the chronologies of glacier advances have shed some light on the nature of glaciation in this region of Central Asia. In the first published work using surface exposure dating in the Kyrgyz Tian Shan, Koppes et al. (2008) studied six glaciated valleys along two generally E–W transects, mainly in the north–central and southern Kyrgyz Tian Shan (Fig. 1B); glaciers in the easternmost Kyrgyz Tian Shan were not dated. Koppes et al. (2008) found that glaciers along the north–central transect advanced to maximum positions during MIS 5 (130 ka–71 ka) and MIS 4 (71 ka–57 ka), whereas glaciers in the south were last at their maximum during MIS 3 (57–29 ka) (Lisiecki and Raymo, 2005). Zech (2012) used cosmogenic dating of boulders from three moraines in the Atbashi Range (Fig. 1B) in south-central Kyrgyzstan (ca 50 km southwest of the MIS 3 sites of Koppes et al., 2008) and presented ages of ca 15, 21 and >56 ka. The mapping and chronological control presented in Koppes et al. (2008) and Zech (2012) largely support limited glaciation of the Kyrgyz Tian Shan during the LGM. Narama et al. (2009, 2007) used OSL dating to reconstruct chronologies of glacial expansion based on moraines mapped in the Terskey Ala Tau and Atbashi ranges in the central Kyrgyz Tian Shan (Fig. 1B), and concluded that evidence exists for expansions of up to 10 km down-valley from current glacier margins in the Terskey Ala Tau during MIS 4 and MIS 2 (LGM), and for expansions up to 15 km down-valley from current glaciers in the Atbashi Range during MIS 3 and MIS 2. In both cases glaciers during the older glaciation were more extensive than during the LGM. We note, however, that exposure ages in Koppes et al. (2008) for moraines in the Ala Bash catchment in the Terskey Ala Tau are significantly older (MIS 4 to MIS 5-6) than corresponding OSL ages in Narama et al. (2009, 2007). Further southwest in Kyrgyzstan, Abramowski et al. (2006) used ^{10}Be surface exposure dating for glacial deposits in two sites in the Alay–Turkestan Range to constrain glacial advances in the area. Minimum apparent exposure ages suggest glacial advances consistent with the record reported in Zech (2012), during MIS 4 or 3, LGM and Lateglacial. The Late Pleistocene glaciers studied by Abramowski et al. (2006) in the Alay–Turkestan Ranges only show evidence for valley glaciation. In sum, these reconstructions are all consistent with valley glacier expansions rather than extensive ice sheet glaciation.

Despite these studies there is still very limited absolute age control for glacial landforms in the Kyrgyz Tian Shan, in particular for the eastern part of the range. Considerable uncertainty remains as to the timing of glacier expansions in this area compared to global and regional records, as well as the degree of spatial variation along the Tian Shan in the timing and relative extent of glacier expansions.

2. Methods

We investigated the timing and extent of past glaciation in the Inylchek and Sary-Dzaz valleys using *in situ* cosmogenic ^{10}Be and ^{26}Al.We first identified and mapped glacial deposits using remote sensing techniques. As part of our fieldwork we checked the mapping in the areas visited, and then collected samples for preliminary cosmogenic dating to constrain the chronology.

2.1. Preliminary mapping of deposits and field observations

Initial mapping of glacial landforms at a scale of 1:1,100,000 was accomplished as part of a larger study (Stroeven et al., 2013). Glacial valleys, marginal moraines, glacial lineations, hummocky terrain, and relict meltwater channels were all mapped. The Stroeven et al. (2013) map was used as a starting point for more detailed mapping of the field area based on the same landform definitions (Fig. 2). Field reconnaissance was used to check the mapping at locations where samples were taken for surface exposure dating.

2.2. Field sampling procedures

Large boulders of quartz-bearing rock types located along moraine crests (where possible) were selected for sampling at each site. Care was taken to minimize potential effects of exhumation or erosion or potential snow cover on each sample. Samples were collected with hammer and chisel from areas on each boulder judged to be the most stable based on continuity and darkness of rock varnish. Surfaces with evidence for spalling were avoided. Location, elevation, sample thickness, boulder geometry, surface dip and dip direction, and topographic shielding measurements were recorded. Key sample data are provided in Table 1 and sample descriptions are included in the Appendix.

2.3. Laboratory methods

Samples were first crushed and sieved to 250–500 μm. Quartz was isolated using standard procedures modified from those of Kohl and Nishiizumi (1992). After checking the resulting purity by measuring major ion concentrations via Inductively Coupled Plasma – Optical Emission Spectroscopy (ICP–OES), the samples were dissolved and Be and Al were isolated using standard anion and cation exchange column procedures (e.g., Strelow et al., 1972; Ochs and Ivy-Ochs, 1997). Resulting Be- and Al-hydroxides were combusted to BeO and Al_2O_3, mixed with Nb and Ag powders, respectively, and pressed into target holders for analysis by accelerator mass spectrometry at PRIME Lab.

2.4. Exposure age calculations

Minimum apparent exposure ages were calculated assuming an absence of boulder surface erosion (based on sampling from stable, varnished surfaces), using a version of the CRONUS online calculator modified to use the northeastern North American production rate for ^{10}Be (3.85 ± 0.19 ^{10}Be at g^{-1} yr^{-1}) with a corresponding ^{26}Al

Table 1
Sample information and ^{10}Be and ^{26}Al results.

Sample	PRIME ID	Location °N/°E	Altitude m a.s.l.	Sample thickness cm	Topographic shielding factor	Quartz g	Be Carrier mg	^{10}Be/^{9}Be × 10^{-15}	[^{10}Be] 10^5 at g^{-1}	^{10}Be age ka	Total Al mg	^{26}Al/^{27}Al × 10^{-15}	[^{26}Al] 10^5 at g^{-1}	^{26}Al age ka
INK-01[a]	201102717	42.02238/79.07863	2669	5	0.973	13.207	0.1044	812.0 ± 40.1	4.534 ± 0.217	17.0 ± 1.2	2.510 ± 0.050	660 ± 210	27.994 ± 8.907	15.6 ± 5.1
INK-01B[a]	201102718	42.02238/79.07863	2669	6	0.973	11.910	0.1066	950.0 ± 24.9	6.016 ± 0.162	22.3 ± 1.3	2.190 ± 0.044	970 ± 90	39.812 ± 3.694	21.9 ± 2.3
INK-02[a]	201102719	42.0227/79.08328	2686	4	0.973	11.382	0.1200	930.0 ± 38.1	6.936 ± 0.278	24.9 ± 1.6	2.198 ± 0.044	940 ± 90	40.513 ± 3.879	21.7 ± 2.4
TS12-IN-01[b]	201203677	42.18686/79.52022	2808	2	0.984	15.397	0.2485	429.7 ± 17.2	4.813 ± 0.206	15.9 ± 1.0	3.658 ± 0.073	640 ± 30	33.934 ± 1.591	16.6 ± 1.1
TS12-IN-02[b]	201203678	42.18691/79.52015	2809	2	0.984	15.837	0.2544	412.3 ± 13.0	4.591 ± 0.159	15.2 ± 0.9	3.534 ± 0.071	630 ± 50	31.373 ± 2.490	15.4 ± 1.4
TS12-IN-03[b]	201203679	42.18684/79.52007	2808	2	0.985	15.104	0.2570	407.6 ± 32.4	4.805 ± 0.398	15.9 ± 1.5	3.164 ± 0.063	680 ± 50	31.793 ± 2.338	15.6 ± 1.4
TS12-IN-04[c]	201203680	42.18844/79.52195	2807	2	0.984	1.112	0.7232	64.3 ± 23.9	6.237 ± 2.930	20.4 ± 9.7	–	–	–	–
TS12-IN-05[b]	201203681	42.19098/79.52985	2830	2	0.987	15.358	0.2571	412.6 ± 19.5	4.788 ± 0.240	15.6 ± 1.1	3.210 ± 0.064	680 ± 30	31.721 ± 1.399	15.3 ± 1.0
TS12-IN-06[c]	201203682	42.19705/79.52792	3003	3	0.984	2.643	0.7273	64.0 ± 9.3	2.627 ± 0.504	7.9 ± 1.6	–	–	–	–
TS12-IN-07[b]	201203683	42.01843/79.07118	2629	3	0.995	15.721	0.2567	596.8 ± 68.5	6.818 ± 0.803	24.6 ± 3.2	3.739 ± 0.075	830 ± 40	44.057 ± 2.123	23.7 ± 1.7
TS12-IN-08[c]	201203684	42.01590/79.06976	2626	2	0.989	0.336	0.7423	23.2 ± 2.0	4.223 ± 1.480	15.7 ± 5.6	–	–	–	–
TS12-IN-09[b]	201203685	42.02038/79.08981	2798	2	0.996	15.555	0.2575	2117.3 ± 59.7	24.892 ± 0.750	80.4 ± 4.7	3.143 ± 0.063	3650 ± 140	164.619 ± 6.314	80.1 ± 5.2
TS12-IN-10[d]	201203686	42.02062/79.08950	2799	5	0.996	19.841	0.2598	2197.8 ± 24.4	20.427 ± 0.308	67.4 ± 3.5	4.369 ± 0.087	2910 ± 110	143.003 ± 5.406	71.0 ± 4.6
TS12-IN-11[d]	201203687	42.02276/79.08514	2690	2	0.972	15.147	0.2560	488.9 ± 11.0	5.735 ± 0.148	20.5 ± 1.1	3.249 ± 0.065	1120 ± 70	53.618 ± 3.351	28.0 ± 2.3
TS12-IN-12[d]	201203688	42.01901/79.07893	2652	2	0.994	15.089	0.2525	999.2 ± 39.4	11.778 ± 0.486	41.2 ± 2.7	3.366 ± 0.067	1430 ± 80	71.205 ± 3.984	37.3 ± 2.8
TS12-SD-01[d]	201203689	42.35397/79.42948	3150	4	0.989	15.204	0.2531	787.5 ± 15.7	9.199 ± 0.210	24.3 ± 1.3	3.863 ± 0.077	1040 ± 40	58.972 ± 2.268	23.2 ± 1.5
TS12-SD-02[d]	201203690	42.35219/79.42641	3136	2	1.000	15.235	0.2514	991.5 ± 16.4	11.523 ± 0.228	29.6 ± 1.6	3.440 ± 0.069	1570 ± 90	79.114 ± 4.535	30.2 ± 2.3
TS12-SD-03[d]	201203691	42.3911/79.44303	3142	3.5	0.993	15.750	0.2530	778.0 ± 12.1	8.767 ± 0.167	23.1 ± 1.2	3.483 ± 0.070	1210 ± 70	59.720 ± 3.455	23.4 ± 1.8
SJ-Q1-1[e]	201300928	41.96749/79.10616	2881	5	1.000	67.210	0.3102	2943 ± 76.3	51.563 ± 1.433	160.3 ± 9.5	–	–	–	–
SJ-Q1-4[e]	201300931	41.97529/79.10931	2845	2	1.000	60.630	0.3104	1412.2 ± 142.3	38.239 ± 3.874	118 ± 13.7	–	–	–	–
SJ-Q1-5[e]	201300932	41.97283/79.11698	2867	2	0.984	40.300	0.3108	266.1 ± 17.2	6.846 ± 0.452	21.5 ± 1.8	–	–	–	–

Notes: All ages calculated assuming an absence of boulder surface erosion, implying a minimum age for the results. Assumed rock density of 2.65 g cm^{-3}. Propagated uncertainties include error in blank, carrier mass, and counting statistics, reported at the1σ level. Be and Al apparent exposure ages calculated using a modified version of the CRONUS-Earth online calculator (Balco et al., 2008), version 2.2, using Balco et al. (2009) northeastern North America ^{10}Be production rates (Lm scaling) $P_{SLHL} = 3.85 \pm 0.19$ at g_{qtz}^{-1} yr^{-1}. ^{10}Be isotope ratios normalized to ^{10}Be standards prepared by Nishiizumi et al. (2007) with a value of 2.85 × 10^{-12}, using a ^{10}Be half-life of 1.36 × 10^6 yr ^{26}Al isotope ratios normalized to ^{26}Al standards prepared by Nishiizumi (2004) with a value of 4.694 × 10^{-12}, using a half-life of 7.05 × 10^5 yr. ^{26}Al production rates calculated from ^{10}Be production rates assuming a ^{26}Al/^{10}Be production ratio of 6.75 (Nishiizumi et al., 2007).

[a] INK samples – Blank of 647,000 ± 250,000 at g^{-1} carrier (0.2149 g, 1069 ppm Be, 9.06 ± 3.49 × 10^{-15} ^{10}Be/^{9}Be) was used for background correction.

[b] TS12-IN-01,2,3,5,7,9 samples – Blank of 874,000 ± 161,000 at g^{-1} carrier (0.2575 g, 1069 ppm Be, 12.2 ± 2.3 × 10^{-15} ^{10}Be/^{9}Be) was used for background correction.

[c] TS12-IN-04, 6, 8 samples – Extremely low quartz content. Blank of 244,000 ± 56,000 at g^{-1} carrier (0.7351 g, 280 ppm Be, 13.0 ± 3.0 × 10^{-15} ^{10}Be/^{9}Be) was used for background correction.

[d] TS12-IN-10, 11, 12 and SD-01,2,3 samples – Blank of 993,000 ± 321,000 at g^{-1} carrier (0.2514 g, 1069 ppm Be, 13.9 ± 4.5 × 10^{-15} ^{10}Be/^{9}Be) was used for background correction.

[e] SJ samples not blank corrected due to extremely large Be content, far in excess of carrier added (SJ-Q1-1: 1.7622 mg Be; SJ-Q1-4: 2.4569 mg Be; SJ-Q1-5: 1.5517 mg Be).

production rate of 25.97 ± 1.30 ^{26}Al at g^{-1} yr^{-1} (Balco et al., 2008, 2009) (Table 1). We prefer the former rate because most estimates of ^{10}Be production rates published since Balco et al. (2009), with broad geographic coverage, generally agree within uncertainties with those values (e.g., Putnam et al., 2010; Fenton et al., 2011; Goehring et al., 2011; Kaplan et al., 2011; Briner et al., 2012; Young et al., 2013). Recent analysis by Heyman supports this as well (Heyman, 2014).

We report ages using the time-dependent Lal (1991)/Stone (2000) scaling model (Lm of Balco et al., 2008). To ensure valid comparisons with the data of Koppes et al. (2008) and Zech (2012), we recalculated those datasets using the same methods (Table S1).

Uncertainties involved in scaling the Balco et al. (2009) production rate to the latitudes of this study are generally minimal, since the calibration is from similar latitudes. However, altitude scaling involves more uncertainty, since published production rate scaling models differ most in their predictions of how the cosmic ray flux varies with altitude. Balco et al. (2008) implement the temporally and spatially varying geomagnetic framework of Lifton et al. (2008) for the scaling models of Dunai (2001) (Du), Desilets and Zreda (2003) (De), and Lifton et al. (2005) (Li). The portion of this framework from 0 to 7 ka includes both latitudinal and longitudinal variation, while Balco et al. (2008) only implement a zonally varying version for the Lm model. A potential exists for both altitudinal and longitudinal uncertainties in the exposure ages, although altitude effects are likely the dominant source of uncertainty. For example, Du, De, and Li all predict a more rapid increase in production rate with altitude than the Lm model, resulting in exposure ages on the order of 5% lower than those predicted by Lm for Lateglacial and LGM ages, increasing to ca 8–12% lower than Lm for MIS 5-6 ages. A more recent scaling model and geomagnetic framework by Lifton et al. (2014) generally agrees with Lm scaling predictions at the latitudes and altitudes considered here, but incorporates a more detailed geomagnetic treatment.

Where more than three samples from the same landform agree within 2σ analytical uncertainty, we calculate inverse *relative*-error-weighted means. We weight the data by relative uncertainties (uncertainty/concentration) because absolute uncertainty tends to increase with increasing concentration. This avoids the potential to skew a traditional inverse error-weighted mean toward lower concentrations. Uncertainties on calculated means are taken as the larger of the error on the weighted mean or the weighted average variance (Bevington and Robinson, 1992).

2.5. Equilibrium line altitudes (ELAs)

Using the SRTM DEM (Jarvis et al., 2008), we performed a preliminary evaluation of *relative* changes in ELA depressions (ΔELA) during the LGM across the Tian Shan, in selected valleys where LGM glacial advances have been constrained by ^{10}Be or OSL dating (Fig. 3). Each ELA was estimated using the toe-to-summit altitude method (TSAM, Benn and Lehmkuhl, 2000) by calculating the mean elevation between the highest peak within the glacier catchment and the terminus of each glacier at a certain period (Benn and Lehmkuhl, 2000). Previous studies have demonstrated that the TSAM-derived ELAs yield similar results as observational ELAs for small valley glaciers in Central and High Asia (Benn and Lehmkuhl, 2000).

3. Results

3.1. Geomorphic observations

The Inylchek Valley below the current glacier is a long, linear, and ca1 km deep valley that has short tributary valleys on the north side draining the southern slope of the Sary-Dzaz Range with small glaciers that are restricted to the highest regions (Fig. 1C). Pervasive fluvial incision in the tributary valleys is evident from incised and faulted tributary fans with ca 10–50 m fluvial scarps. Fluvial deposits along the main valley also show evidence of multiple depositional and/or incision events, with 3–4 terraces common throughout both the Inylchek and Sary-Dzaz valleys. The Inylchek Valley has glacially smoothed bedrock extending up to ca 800 m above the present valley floor on both sides. A series of prominent discontinuous moraines and lateral meltwater channels (that accentuate the ridged relief) is present on the lower slopes of the northern side of upper Inylchek Valley (Figs. 1C, 2A and 4A). The moraines are sub-parallel to the main valley direction, occur up to ~200 m above the valley floor, and are partly covered by the present sandur deposits at the valley floor. The lateral formations extend into a terminal moraine complex above the lower Inylchek Valley at the junction with the Sary-Dzaz River (Figs. 1C, 2B and 4B). Numerous large granitic boulders that appear well suited for cosmogenic nuclide sampling are present on some of these moraines (Fig. 4C). Offset tributary streams draining the south side of the Sary-Dzaz Range provide evidence of recent, generally left-lateral, fault slip.

The broad valley of the Sary-Dzaz River north of the Sary-Dzaz Range exerts strikingly different topographic control of its glacial geomorphology than that in the Inylchek Valley. In contrast to the generally short tributaries on the north slope of the Inylchek Valley (~3 km), the tributary valleys on the other side of the Sary-Dzaz Range are ~15–20 km from headwaters to junctions with the main river. There is also evidence of extensive glaciation in the Sary-Dzaz Valley in the form of glacially molded bedrock surfaces (Fig. 4E) extending ca 300 m above the present valley floor (note

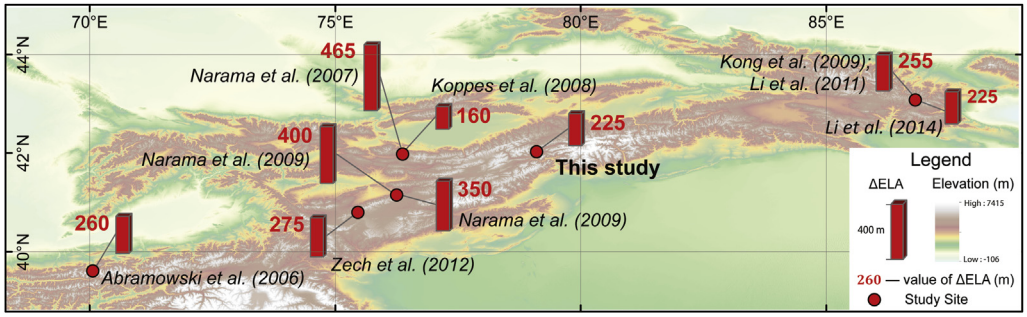

Fig. 3. Equilibrium-line altitude depressions (ΔELAs) for the LGM (MIS 2) in the Tian Shan from the studies indicated. ΔELAs were calculated using the TSAM method (see text for details). The studies utilizing ^{10}Be for moraine age control show only limited relative ΔELA variation along the range, while the OSL-dated moraines of Narama et al. (2007, 2009) yield much larger ΔELAs – note in particular the discrepancy at the Terskey Ala Tau site of both Narama et al. (2007) and Koppes et al. (2008). See text for discussion of this discrepancy.

Fig. 4. Site photographs. A) Looking east along a low moraine adjacent to Inylchek River in the upper Inylchek Valley. People for scale standing on boulder TS12-IN-05 (Fig. 2A). B) Looking west from intermediate-age marginal moraine ridge immediately south of the terminal moraine complex at the west end of Inylchek Valley, toward boulders TS12-IN-09 and -10 (Fig. 2B). A hummocky deposit within the terminal moraine complex is visible to the right of center, with multiple outwash terrace levels left of center of photograph. C) Boulder INK-01 on the crest of the main marginal moraine in the terminal moraine complex at the west end of Inylchek Valley (Fig. 2B). D) High moraine ridge remnant south of Inylchek Valley along the east side of the Sary-Dzaz River, looking south, near SJ-Q1-1 (Fig. 2C). E) Looking west from the eastern portion of the Sary-Dzaz Valley, along the reach of the Sary-Dzaz River incised into bedrock. Note the hummocky till deposits draped over bedrock and general lack of surface boulders. F) Looking south from site TS12-SD-03 (Fig. 2D) – an erratic boulder perched on a roche moutonnée along the north side of the Sary-Dzaz River. Note the multiple fluvial terraces and streamlined hummocky forms, and, again, the lack of surface boulders. Sary-Dzaz Range in the distance. G) Looking south from the confluence of the Semyonov and Mushketov valleys in the upper Sary-Dzaz Valley. Note the numerous terrace levels and bedrock incision. H) Boulder TS12-SD-01 looking north to the Sary-Dzaz River (Fig. 2D). Note the subdued upland topography in the distance.

that the Sary-Dzaz Valley floor is ca 500 m higher in altitude than the Inylchek Valley floor, so maximum ice surfaces appear consistent between both valleys). A key difference between the valleys is that the Sary-Dzaz Valley floor is blanketed with hummocky moraine, with evidence of glacial streamlining (Fig. 4F). The upper limit of the hummocky moraine is marked by lateral moraines, some of which are broad and continuous, while others are more segmented, partly due to incision of marginal meltwater channels (Fig. 2D). In contrast to Inylchek Valley, there are only sparse surficial boulders appropriate for cosmogenic nuclide sampling in the Sary-Dzaz Valley. As with the Inylchek Valley, the Sary-Dzaz Valley contains 3–4 distinct fluvial terrace levels. However, numerous additional stream terraces and areas of bedrock incision occur in the upper Sary-Dzaz Valley near the confluence of the Semyonov and Mushketov valleys in an area where two active faults intersect (Mikolaichuk et al., 2008) (Fig. 4G).

3.2. Exposure ages

Analytical results are presented in Table 1. All quoted uncertainties are at the 1σ level, unless otherwise indicated. Samples TS-IN-04, -06, and -08 all had very small quartz yields (ca 1%). As a result, they have correspondingly large uncertainties and were only analyzed for ^{10}Be. Samples INK01 and INK01b were collected as a pair from the top center and top edge, respectively, of a large blocky boulder (Fig. 4C) as a test of edge versus center effects (e.g., Masarik and Wieler, 2003; Lal and Chen, 2005). No debris or other evidence for major spalling or erosion was noted on the flat top of this boulder, although INK01 exhibited somewhat darker varnish than INK01b. Consistent results for both ^{10}Be and ^{26}Al in both samples yielded a lower concentration at the top center of the boulder than at the top edge, in contrast to the theoretical prediction of lower concentrations at the edge. This indicates that surface erosion of the boulder at sampling location INK01 has likely affected cosmogenic nuclide concentrations, in contrast to what might be expected from the differing degrees of varnish (Table 1). We do not consider sample INK01 further in this analysis, but retain sample INK01b.

3.3. Inylchek Valley

Boulder samples were collected at three sites in the Inylchek valley (Fig. 2A–C). Below we discuss results from each of these sites.

3.3.1. Lateral moraine up-valley

A series of prominent lateral moraines and meltwater channels were investigated along the north side of the Inylchek River, approximately 10 km west of the current front of the Southern Inylchek Glacier (Fig. 2A). Samples TS12-IN-01 through TS12-IN-05 were collected from large granitic boulders situated along the crest of the lowermost moraine ridge, up to 35 m above the modern sandur (Figs. 2A and 4A). Results from these samples are tightly clustered (Table 1) with an inverse relative-error-weighted mean minimum apparent exposure age of 15.6 ± 0.5 ka for ^{10}Be (n = 5, including TS12-IN-04) and 15.8 ± 0.7 ka for ^{26}Al (n = 4).

Sample TS-IN-06 was collected from a ca 1.5 m diameter granitic boulder at the uppermost moraine level (Fig. 2A), approximately 200 m above the lowest moraine ridge. In the area investigated, this level consisted of three sub-parallel moraine ridges with limestone and granitic boulders (typically <1 m in diameter). This sample was collected from the uppermost of the three moraine ridges, closest to the mountain front, and so one would expect it to be older than moraine ridges lower down on the same slope. The apparent exposure age for this sample of 7.9 ± 1.6 ka (Fig. 2A) indicates it is significantly and anomalously younger than suggested by its geomorphological position above samples TS12-IN-01 through TS12-IN-05 (see above). Processes that can lead to anomalously young exposure ages include shielding by sediment during post-depositional exhumation of a boulder, and significant boulder surface erosion (Heyman et al., 2011b). This boulder was darkly varnished, suggesting a long period of surface exposure at some time in its history, and had no evidence of recent surficial spalling or erosion. Its granitic composition indicates glacial transport from a source up-valley, as opposed to a more local source such as the adjacent glacially molded limestone bedrock. Alternatively, analysis in Google Earth and high-resolution CORONA satellite imagery now in the public domain (frame DS1112-2201DA037_a, 12/1970: http://eros.usgs.gov/satellite-imagery) indicates that the surface from which TS-IN-06 was collected may have been disturbed by mass movement (not readily evident in the field), perhaps associated with movement along the Atbashi-Inylchek fault. This was the only sample collected from this surface, and its relationship to the time of moraine deposition is questionable, so we exclude this sample from further analysis.

3.3.2. Terminal moraine complex

The western end of the Inylchek Valley contains a significant terminal moraine complex at the junction of the Inylchek and Sary-Dzaz rivers, enclosing a large, steep-sided deposit with a broad, hummocky top surface likely indicative of past stagnant ice (Figs. 2B and 4C). The moraine has been breached by the Sary-Dzaz River, which has also cut into the north and west sides of the hummocky deposit. Several smaller moraine ridges lie outboard of that moraine to the south (Fig. 2B), while at least three outwash terrace levels are present downstream of the terminal moraine (Fig. 4B). In addition, a high lateral moraine ridge is present on the southern (north-facing) slope of Inylchek Valley as it turns south, approximately 130 m above the terminal moraine (Figs. 2B and 4B). Each moraine in this complex contains large boulders along its crest and slopes; these boulders are up to several m in diameter (Fig. 4C). The large size of most of these boulders and the generally high clast content in the moraines minimizes the possibility of moraine degradation effects such as those modeled by Putkonen and Swanson (2003), particularly for the younger moraines considered. Boulders along the lower slopes of the innermost terminal moraine almost uniformly exhibit a dark reddish varnish, and appear significantly more weathered than boulders on the upper slopes of the same moraine. This contrast indicates that a younger moraine may have been deposited atop an earlier moraine.

Samples INK-01b (Fig. 4C), INK-02, and TS12-IN-07 and -11 were collected from boulders along the crest of the innermost terminal moraine, and their ^{10}Be and ^{26}Al apparent exposure ages cluster at 22.5 ± 2.0 ka (n = 4) and 24.3 ± 2.8 ka (n = 4), respectively (Table 1; Fig. 2B). Samples TS12-IN-08 and -12 are from boulders on two crests outside of the main terminal moraine. TS12-IN-08 yielded a ^{10}Be apparent exposure age of 15.7 ± 5.6 ka, overlapping the mean age of the terminal moraine at 2σ, while TS12-IN-12 provided consistent ^{10}Be and ^{26}Al apparent exposure ages of 41.2 ± 2.7 ka and 37.3 ± 2.8 ka, respectively (Table 1). TS12-IN-09 and -10 were collected from two very large boulders on the high lateral ridge (Fig. 4B), and gave significantly older and consistent apparent exposure ages of 80.4 ± 4.7 ka (^{10}Be) and 80.1 ± 5.2 ka (^{26}Al), and 67.4 ± 3.5 ka (^{10}Be) and 71.0 ± 4.6 ka (^{26}Al), respectively (Table 1).

3.3.3. Highest moraine remnant

Approximately 5 km south of the Inylchek Valley terminal moraine complex, just north of the junction of the Kaindy Valley with the Sary-Dzaz River (Fig. 1C), is a lateral moraine remnant approximately 400 m above the modern river (ca 80 m higher

altitude than the high lateral ridge described above) (Fig. 2C). Samples from three large boulders were collected and analyzed for ^{10}Be: SJ-Q1-1, -4, and -5. Sample SJ-Q1-1 was taken from a large granite boulder found in close association with the lateral moraine remnant on the valley slope (Fig. 4D). Samples SJ-Q1-4 and -5 were from granite erratics on a high bench at a similar elevation to the moraine. They were not part of a moraine crest but are nonetheless interpreted as indicative of an ice surface elevation similar to the ice surface depositing the lateral moraine remnant. These three samples were unusual in that they had total Be content in solution well in excess of the Be added as a carrier (see notes, Table 1). This anomaly indicates that an accessory beryllium-bearing phase was not completely removed during pretreatment. However, this excess Be did not degrade our precision because these high-altitude samples still had significant ^{10}Be inventories. Minimum apparent exposure ages derived from these samples were highly scattered ranging from 160.3 ± 9.5 ka for the boulder associated with the moraine remnant (SJ-Q1-1) to 118 ± 13.7 (SJ-Q1-4) and 21.5 ± 1.8 ka (SJ-Q1-5) for the dispersed erratics, indicating either potential inheritance in the oldest sample and/or significant erosional modification or more recent downslope movement of the boulders with the younger apparent ages.

3.4. Sary-Dzaz Valley

The portion of the upper Sary-Dzaz Valley that was readily accessible by road was characterized by hummocky till deposits grading into glacially streamlined bedforms (including a few drumlins) (Figs. 2C, 4E, 4F), and a striking scarcity of surface boulders available for sampling (particularly compared to the Inylchek Valley glacial deposits). Granitic boulders were common within the hummocky till deposits, as noted in river cuts, but rare at the surface. Two large granite boulders were sampled from moraine ridge surfaces marking the upper margin of the hummocky deposits: TS12-SD-01 and -02 (Fig. 4H). A third sample (TS12-SD-03) was collected from a large granite erratic boulder atop a granitic roche moutonnée on the north side of the Sary-Dzaz River. Apparent exposure ages from ^{10}Be and ^{26}Al agree within uncertainties for each sample, ranging from approximately 23 ka for TS12-SD-01 and -03 to approximately 30 ka for TS12-SD-02 (Table 1).

4. Discussion

The Inylchek and Sary Dzaz valleys provide evidence for an expansion of valley glaciers during the LGM (Table 1, Fig. 5). Compared to present-day glacier margins, LGM ice advanced ca 60 km down the Inylchek and Sary-Dzaz valleys, consistent with a calculated ELA depression of 225 m. The preservation of even older lateral moraine segments (samples TS12-IN-09, -10, and SJ-Q1−1, -4, and -5) down-valley and at higher elevations than the LGM Inylchek terminal moraine complex, taken together with our ages, support the limited LGM ice expansion hypothesis of Bondarev (1976).

ELA depressions calculated for the Tian Shan during the LGM range from 160 to 465 m (Fig. 3). This range in ELA depressions is similar to that derived for the Tian Shan by Heyman (2014) using the toe-to-headwall altitude ratio (THAR) method and only ^{10}Be-

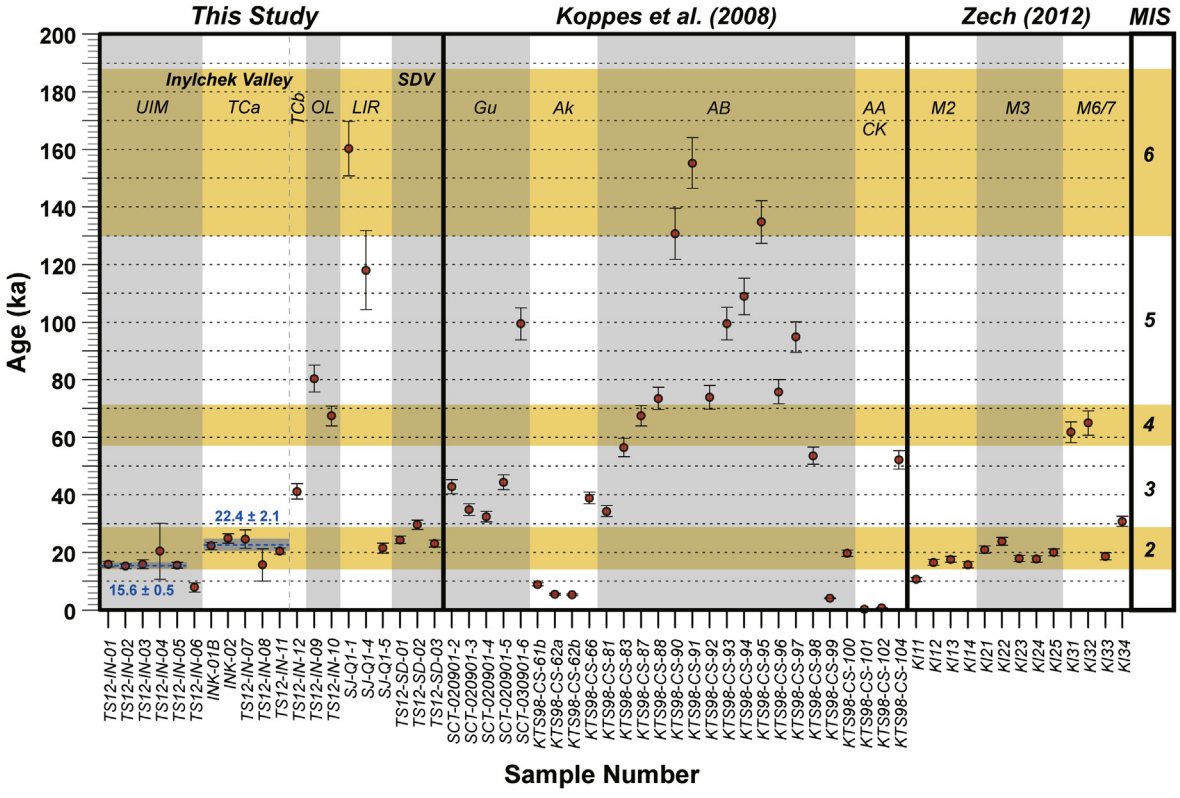

Fig. 5. Comparison of apparent ^{10}Be exposure ages from Inylchek/Sary-Dzaz valleys with recalculated Koppes et al. (2008) and Zech (2012) apparent ^{10}Be exposure ages (Table 1 and S1 in the appendix). Approximate MIS boundaries in gold from Lisiecki and Raymo (2005). Site abbreviations: UIM = Upper Inylchek moraines; TC = Terminal moraine complex, TCa = main ridge, TCb = ridge outboard of main ridge; OL = Older lateral moraine; LIR = Lower Inylchek remnant; SDV = Sary-Dzaz Valley. Koppes et al. (2008) site abbreviations: Gu = Gulbel; Ak = Aksai; AB = Ala Bash; AA = Ala Archa; CK = Chor Kyrchak. Blue dashed lines and shading around the UIM and TCa samples indicate inverse relative-error-weighted means for each landform. TS12-IN-08 is included in the TCa weighted mean. Excluding that sample does not change the mean value or uncertainty significantly (22.5 ± 2.0 ka).

based estimates of terminal moraine age. Estimates of ΔELAs from moraines dated by Narama et al. (2007, 2009) using OSL are consistently and significantly larger (350–465 m) than those for LGM moraines with ^{10}Be age control (160–275 m), even from the same catchment (Fig. 3). However, moraines from the Ala Bash catchment in the Terskey Ala Tau that Narama et al. (2007) concluded were LGM based on OSL dating appear to be MIS 4 or older based on ^{10}Be ages presented in Koppes et al. (2008) (Section 1.2; Table S1). This variability between methods needs to be investigated in more detail because it has important implications for understanding how these glaciers differ in their responses to global and regional climate change. As such, we restrict further discussion to sites with cosmogenic nuclide age control, which exhibit a relatively narrow LGM ΔELA range of 160–275 m.

The LGM extents of glaciers in the Inylchek and Sary Dzaz valleys appear to contrast with the results of Koppes et al. (2008) who found no evidence for significant LGM glacier expansion in north–central and southern areas of the Kyrgyz Tian Shan. We note, however, that their dating was of a reconnaissance nature, and thus they may not have mapped and dated relatively minor LGM advances. In addition, the glaciers in the catchments studied by Koppes et al. (2008) were much smaller than those in the Inylchek and Sary Dzaz valleys and thus their responses to climate deterioration during the LGM would tend to be more limited than the large glaciers in this study. The Inylchek and Sary Dzaz records are consistent with evidence from the Atbashi Range for LGM and Lateglacial ice expansion (Zech, 2012) (Fig. 1). The available evidence thus indicates moderate spatial variation in glacier extent during the LGM along the length of the Kyrgyz Tian Shan (the lowest ΔELA values were from the central part of the range: 225 m from this study, and 160 m at the Ala Bash site of Koppes et al. (2008)). The modest relative variation in ΔELAs at the LGM within the Kyrgyz Tian Shan likely reflects regional climatic influences modulated by local factors such as relief, aspect, and degree of debris cover on each glacier, as well as corresponding sensitivities of glacier mass balances to temperature and precipitation (e.g., Zech et al., 2008; Rupper et al., 2009; Zech et al., 2013; Heyman, 2014; Owen and Dortch, 2014).

The Inylchek Valley mapping and chronology also include evidence for Lateglacial and pre-LGM ice advances. Taken at face value, the latter may have occurred during MIS 3, MIS 4, MIS 5 and/or MIS 6 (ca 130–188 ka, Lisiecki and Raymo, 2005), or even earlier, but the limited number of exposure ages and the scatter in those ages prohibit a more robust interpretation (Fig. 5). Consistent Lateglacial ages were found on a low moraine along the north bank of the Inylchek River approximately 10 km down-valley from the current glacier snout (Table 1, Figs. 2A and 4), corresponding with the Atbashi Lateglacial ages of Zech (2012) but contrasting with Koppes et al. (2008) who did not note evidence of Lateglacial glacier expansion in north–central and southern areas of the Kyrgyz Tian Shan. Both Koppes et al. (2008) and our study provide evidence for glacial deposits in the Kyrgyz Tian Shan that predate the LGM.

The terminal moraine complex at the west end of Inylchek Valley contains the most complete record of glacial events in the study area, including an innermost MIS 2 moraine and a potential MIS 3 moraine ridge just outside of that. In close association but at somewhat higher elevation we dated an MIS 4 or 5 remnant along the southern valley wall as it turns south, and finally a significantly higher moraine remnant further south along the eastern side of the Sary-Dzaz River north of the Kaindy Valley (the next valley south of Inylchek) (Figs. 1–3, Table 1). The minimum apparent exposure ages of the older lateral moraine ridges correlate quite well with the age assessment of 50–60 ka in Dikikh et al. (1991) (see Section 1.2) that was based on stratigraphic correlation between terraces and moraines. The dates given here for glacial landforms in the middle section of the valley do not correspond with an age estimate of 25–35 ka from Dikikh et al. (1991) but correlate reasonably well with three ^{10}Be exposure ages from a moraine in the Atbashi Range that have a weighted mean apparent exposure age of 16.7 ± 1.0 ka (Table S1) (Zech, 2012). For the oldest deposit we studied, sample SJ-Q1-1 was the only one of the samples directly associated with what is still identifiable as a lateral moraine remnant, although we acknowledge that this age could be affected by nuclide inheritance to an unknown degree. While the scatter in these sample ages indicates that we cannot rigorously constrain the most extensive glaciation recorded in the glacial landforms to better than pre-LGM, the landscape position and degree of likely post-depositional modification of this remnant implies a significantly older glacial expansion – perhaps even predating MIS 5 or 6 as suggested by the two oldest minimum apparent exposure ages.

The data available from the Inylchek and Sary-Dzaz valleys so far indicate a record of glacial advances that include MIS 2 and older events, some of which appear to correspond broadly with cold periods in Northern Hemisphere climate cycles and temperature depression records (e.g., Clark et al., 1999). This is consistent with suggestions of MIS 2, MIS 4, and earlier glaciations in the Pamir region (Abramowski et al., 2006; Owen et al., 2008, 2012; Zech et al., 2013) and on the southeastern Tibetan Plateau (Fu et al., 2013), but contrasts to records from the inner and northern Tibetan Plateau that lack MIS 2 glacier responses (Meriaux, 2004; Owen et al., 2005; Heyman et al., 2011a).

The clearest temporal records from the Inylchek and Sary Dzaz valleys are the well-clustered LGM and Lateglacial ages, which are consistent with the data from Atbashi of Zech (2012). Together with ^{10}Be minimum apparent exposure ages from the easternmost Tian Shan in China (Kong et al., 2009; Li et al., 2011, 2014) and Atbashi in Kyrgyzstan (Zech, 2012), the Inylchek and Sary-Dzaz data indicate more limited glacier advances in the Tian Shan during the LGM than might be expected at times that are broadly synchronous with Northern Hemisphere ice sheet glaciation. A strong Siberian High during the LGM, and thus reduced moisture transport due to weaker Westerlies, has been proposed as an explanation for these observations (Zech, 2012).

Our limited chronological data from the older glacial deposits in the two valleys are harder to interpret without additional samples (Fig. 5) due to greater scatter in ages that straddle MIS boundaries. One could interpret some of the older deposits as corresponding generally with MIS 4 and 6, following Northern Hemisphere ice sheets, or with MIS 3 and 5, out of phase with those ice sheets. Studies by Dortch et al. (2013) in the western Himalaya-Tibetan Plateau region and Murari et al. (2014) in the central and eastern Himalaya find evidence for both Northern Hemisphere climatic influences as well as strong monsoonal signals. A recent study by Cheng et al. (2012) of speleothem δ^{18}O variations from Kesang Cave in the Chinese Tian Shan (ca 180 km northeast of the study area) lends strong support for significant monsoonal influence in the vicinity of this study over the last 500 ka, anti-phased with Northern Hemisphere insolation variations. Indeed, Holocene stable isotopic analyses of sediment cores from Lake Issyk-Kul (ca 120 km west-northwest of our study area – Fig. 1B) seem to indicate an early Holocene monsoonal influence (Ricketts et al., 2001), although other studies (e.g., Chen et al., 2008) indicate a dominant Holocene influence from the Westerlies.

5. Conclusions

Building on previous mapping and relative age dating studies, we present the first absolute dating results for glacial deposits in the Inylchek and Sary-Dzaz valleys draining the highest mountains of the eastern Kyrgyz Tian Shan. These data provide insight that is

relevant for discussions on the extent and timing of former glacier expansions in the Tian Shan, including uncertainty regarding the extent of LGM ice cover, and the degree to which expansions of glaciers in the Tian Shan are synchronous with Northern Hemisphere records of ice sheet glaciation.

Cosmogenic nuclide ^{10}Be and ^{26}Al apparent exposure ages for large boulders on, or associated with, moraines record up to five stages of glaciation, with the most detailed record in this study preserved in Inylchek Valley. As a pilot-scale study with only 21 samples dated (Table 1), our conclusions are tentative at this stage, pending a more detailed study. However, the results to date indicate the presence of:

1. Lateral moraine remnants and meltwater channels in the upper Inylchek valley of Lateglacial age. Apparent exposure ages are tightly clustered with an inverse relative-error-weighted mean of 15.6 ± 0.5 ka for ^{10}Be ($n = 5$) and 15.8 ± 0.7 ka for ^{26}Al ($n = 4$).
2. Moraines in a main terminal moraine complex at the west end of Inylchek Valley of LGM (MIS 2) age, overriding older moraines, and in the Sary-Dzaz Valley.
3. A potential MIS 4 or MIS 5 moraine remnant above the terminal moraine complex along the southern wall of Inylchek Valley.
4. An older and significantly higher moraine remnant further down the main valley after the Sary-Dzaz and Inylchek valleys join has a pre-LGM age, but more likely also predates MIS 5 or 6.

Evidence for the timing and extent of glacial expansion is consistent with the limited ice expansion hypothesis of Bondarev (1976) for this area. The spatial and temporal correlations with glaciations during Lateglacial times and MIS 2 indicate a regional climate change driver for glaciation in this area and a late Pleistocene link to Northern Hemisphere climate oscillations. However, this regional driver is superimposed upon local contexts with variable tectonic and physiographic settings, which may explain different responses or preservation of deposits between adjacent valleys, such as the Inylchek and Sary-Dzaz. Older climatic correlations are more tenuous and await further data.

The data now available point to the possibility of a spatial variation in glacier records along the Tian Shan, and indicate the need for a systematic program of paleoglaciological reconstruction along N–S and E–W transects to explore this pattern and its implications for how regional or global climate changes are reflected along and across mountain ranges.

Acknowledgments

Funding for this research was provided by the Swedish Research Council to Stroeven (No. 2011-4892), and by the National Geographic Society (Grant 9073-12) to Harbor and Lifton, Purdue University and Stockholm University. Heermance, Oskin, and Burbank were supported by NASA grant NAG5-13758. We are grateful to Roland Zech and Jason Dortch for constructive reviews that significantly improved the manuscript. We thank the crew of the helicopter (and E. Kalashnikova personally) who enabled access to key parts of the field area, the staff at the Central Asian Institute of Applied Geosciences, Bishkek, and the German Research Centre for Geosciences, Potsdam, for invaluable assistance. We are indebted to Greg Chmiel for help with ^{10}Be and ^{26}Al sample processing, and PRIME Lab personnel for accelerator mass spectrometry analyses.

Appendix A. Supplementary data

Supplementary data related to this article can be found at http://dx.doi.org/10.1016/j.quascirev.2014.06.032.

References

Abdrakhmatov, K.Y., Aldazhanov, S.A., Hager, B.H., Hamburger, M.W., Herring, T.A., Kalabaev, K.B., Makarov, V.I., Molnar, P., Panasyuk, S.V., Prilepin, M.T., Reilinger, R.E., Sadybakasov, I.S., Souter, B.J., Trapeznikov, Y.A., Tsurkov, V.Y., Zubovich, A.V., 1996. Relatively recent construction of the Tien Shan inferred from GPS measurements of present-day crustal deformation rates. Nature 384, 450–453.

Abramowski, U., Bergau, A., Seebach, D., Zech, R., Glaser, B., Sosin, P., Kubik, P., Zech, W., 2006. Pleistocene glaciations of Central Asia: results from ^{10}Be surface exposure ages of erratic boulders from the Pamir (Tajikistan), and the Alay–Turkestan range (Kyrgyzstan). Quat. Sci. Rev. 25, 1080–1096.

Aizen, V.B., Aizen, E.M., Dozier, J., Melack, J.M., Sexton, D.D., Nesterov, V.N., 1997. Glacial regime of the highest Tien Shan mountain, Pobeda-Khan Tengry massif. J. Glaciol. 43, 503–512.

Aizen, V.B., Aizen, E.M., Kuzmichonok, V.A., 2007. Glaciers and hydrological changes in the Tien Shan: simulation and prediction. Environ. Res. Lett. 2, 045019.

Aleshinskaya, Z.V., 1971. Section of Recent Deposits in Issyk-Kul Depression (in Russian). Moscow State University.

Aleshinskaya, Z.V., Bondarev, L.G., Chigirev, N.V., Shumova, G.M., 1976. About Tectonics, Climate and Glaciations of Tian Shan in Pleistocene (in Russian). In: Problems of Physical Geography and Paleogeography. Moscow State University, Moscow, pp. 198–210.

Arendt, A., Bolch, T., Cogley, J.G., Gardner, A., Hagen, J.-O., Hock, R., Kaser, G., Pfeffer, W.T., Moholdt, G., Paul, F., Radić, V., Andreassen, L., Bajracharya, S., Barrand, N., Beedle, M., Berthier, E., Bhambri, R., Bliss, A., Brown, I., Burgess, D., Burgess, E., Cawkwell, F., Chinn, T., Copland, L., Davies, B., De Angelis, H., Dolgova, E., Filbert, K., Forester, R.R., Fountain, A., Frey, H., Giffen, B., Glasser, N., Gurney, S., Hagg, W., Hall, D., Haritashya, U.K., Hartmann, G., Helm, C., Herreid, S., Howat, I., Kapustin, G., Khromova, T., Kienholz, C., Köonig, M., Kohler, J., Kriegel, D., Kutuzov, S., Lavrentiev, I., Le Bris, R., Lund, J., Manley, W., Mayer, C., Miles, E., Li, X., Menounos, B., Mercer, A., Mölg, N., Mool, P., Nosenko, G., Negrete, A., Nuth, C., Pettersson, R., Racoviteanu, A., Ranzi, R., Rastner, P., Rau, F., Raup, B., Rich, J., Rott, H., Schneider, C., Seliverstov, Y., Sharp, M., Sigurðsson, O., Stokes, C., Wheate, R., Winsvold, S., Wolken, G., Wyatt, F., Zheltyhina, N., 2012. Randolph Glacier Inventory – a Dataset of Global Glacier Outlines: Version 3.2. Global Land Ice Measurements from Space, Boulder Colorado, USA.

Balco, G., Briner, J., Finkel, R.C., Rayburn, J.A., Ridge, J.C., Schaefer, J.M., 2009. Regional beryllium-10 production rate calibration for late-glacial northeastern North America. Quat. Geochronol. 4, 93–107.

Balco, G., Stone, J.O., Lifton, N.A., Dunai, T.J., 2008. A complete and easily accessible means of calculating surface exposure ages or erosion rates from Be-10 and Al-26 measurements. Quat. Geochronol. 3, 174–195.

Benn, D., Lehmkuhl, F., 2000. Mass balance and equilibrium-line altitudes of glaciers in high-mountain environments. Quat. Int. 65, 15–29.

Bevington, P., Robinson, D., 1992. Data Reduction and Error Analysis for the Physical Sciences, second ed. McGraw-Hill, p. 328.

Bolch, T., 2007. Climate change and glacier retreat in northern Tien Shan (Kazakhstan/Kyrgyzstan) using remote sensing data. Glob. Planet. Change 56, 1–12.

Bondarev, L.G., 1976. Influence of Tectonics on Evolution and Formation of Glacial Terrain (in Russian). Ilim, Frunze.

Briner, J.P., Young, N.E., Goehring, B.M., Schaefer, J.M., 2012. Constraining Holocene ^{10}Be production rates in Greenland. J. Quat. Sci. 27, 2–6.

Chedia, O.K., 1986. Tien Shan Morphostructures and Recent Tectogenesis (in Russian). Ilim, Frunze.

Chen, F., Yu, Z., Yang, M., Ito, E., Wang, S., 2008. Holocene moisture evolution in arid central Asia and its out-of-phase relationship with Asian monsoon history. Quat. Sci. Rev. 27, 351–364.

Cheng, H., Zhang, P.Z., Spötl, C., Edwards, R.L., Cai, Y.J., Zhang, D.Z., Sang, W.C., Tan, M., An, Z.S., 2012. The climatic cyclicity in semiarid-arid central Asia over the past 500,000 years. Geophys. Res. Lett. 39.

Clark, P.U., Alley, R.B., Pollard, D., 1999. Northern hemisphere ice-sheet influences on global climate change. Science 286, 1104–1111.

Demchenko, M.A., 1935. The Glaciers of Khan Tengri massif (in Russian). Glacier research in the Soviet Union, pp. 64–86.

Desilets, D., Zreda, M., 2003. Spatial and temporal distribution of secondary cosmic-ray nucleon intensities and applications to *in situ* cosmogenic dating. Earth Planet. Sci. Lett. 206, 21–42.

Dikikh, A.N., Bakov, Y.K., Koshoev, M.K., Melnikova, A.P., Dikikh, L.L., 1991. Ice Resources of Central Tian Shan (in Russian). Ilim, Bishkek, Kyrgyzstan.

Dolgushin, L.D., Osipova, G.B., 1989. Glaciers (in Russian). Mir, Moscow, Russia.

Dortch, J.M., Owen, L.A., Caffee, M.W., 2013. Timing and climatic drivers for glaciation across semi-arid western Himalayan–Tibetan orogen. Quat. Sci. Rev. 78, 188–208.

Dunai, T.J., 2001. Influence of secular variation of the geomagnetic field on production rates of *in situ* produced cosmogenic nuclides. Earth Planet. Sci. Lett. 193, 197–212.

Dyurgerov, M.B., 2010. Reanalysis of Glacier Changes: From the IGY to the IPY, 1960–2008. In: Data of Glaciological Studies, pp. 6–115.

Fenton, C.R., Hermanns, R.L., Blikra, L.H., Kubik, P.W., Bryant, C., Niedermann, S., Meixner, A., Goethals, M.M., 2011. Regional ^{10}Be production rate calibration for the past 12 ka deduced from the radiocarbon-dated Grotlandsura and Russenes rock avalanches at 69° N, Norway. Quat. Geochronol. 6, 437–452.

Fu, P., Heyman, J., Hättestrand, C., Stroeven, A.P., Harbor, J.M., 2012. Glacial geomorphology of the Shaluli Shan area, southeastern Tibetan Plateau. J. Maps 8, 48–55.
Fu, P., Stroeven, A.P., Harbor, J.M., Hättestrand, C., Heyman, J., Caffee, M.W., Zhou, L., 2013. Paleoglaciation of Shaluli Shan, southeastern Tibetan Plateau. Quat. Sci. Rev. 64, 121–135.
Glazirin, G.E., 2010. A century of investigations on outbursts of the ice-dammed Lake Merzbacher (Central Tien Shan). Austrian J. Earth Sci. 103, 171–179.
Goehring, B.M., Mangerud, J., Svendsen, J.I., Schaefer, J., Finkel, R., 2011. Late glacial and Holocene ^{10}Be production rates for western Norway. J. Quat. Sci. 27, 89–96.
Grosswald, M., Kuhle, M., Fastook, J., 1994. Würm glaciation of Lake Issyk-Kul area, Tian Shan Mts.: a case study in glacial history of Central Asia. GeoJournal 33, 273–310.
Häusler, H., Scheibz, J., Leber, D., Kopecny, A., Echtler, H., Wetzel, H.-U., Moldobekov, B., 2011. Results from the 2009 geoscientific expedition to the Inylchek Glacier, Central Tien Shan (Kyrgyzstan). Austrian J. Earth Sci. 104, 47–57.
Heyman, J., 2014. Paleoglaciation of the Tibetan Plateau and surrounding mountains based on exposure ages and ELA depression estimates. Quat. Sci. Rev. 91, 30–41.
Heyman, J., Hattestrand, C., Stroeven, A., 2008. Glacial geomorphology of the Bayan Har sector of the NE Tibetan Plateau. J. Maps 42, 62.
Heyman, J., Stroeven, A.P., Caffee, M.W., Hättestrand, C., Harbor, J.M., Li, Y., Alexanderson, H., Zhou, L., Hubbard, A., 2011a. Palaeoglaciology of Bayan Har Shan, NE Tibetan Plateau: exposure ages reveal a missing LGM expansion. Quat. Sci. Rev. 30, 1988–2001.
Heyman, J., Stroeven, A.P., Harbor, J.M., Caffee, M.W., 2011b. Too young or too old: evaluating cosmogenic exposure dating based on an analysis of compiled boulder exposure ages. Earth Planet. Sci. Lett. 302, 71–80.
Jarvis, A., Reuter, H.I., Nelson, A., Guevara, E., 2008. Hole-filled SRTM for the Globe Version 4 available from the CGIAR-CSI SRTM 90m Database. http://srtm.csi.cgiar.org.
Kachaganov, S., 2011. Geomorphology and Paleogeography of Chon Kemin Catchment Area in Pleistocene (in Russian). Turar, Bishkek, Kyrgyzstan.
Kaplan, M.R., Strelin, J.A., Schaefer, J.M., Denton, G.H., Finkel, R.C., Schwartz, R., Putnam, A.E., Vandergoes, M.J., Goehring, B.M., Travis, S.G., 2011. In-situ cosmogenic ^{10}Be production rate at Lago Argentino, Patagonia: implications for late-glacial climate chronology. Earth Planet. Sci. Lett. 309, 21–32.
Kohl, C., Nishiizumi, K., 1992. Chemical isolation of quartz for measurement of in-situ-produced cosmogenic nuclides. Geochim. Cosmochim. Acta 56, 3583–3587.
Kong, P., Fink, D., Na, C., Huang, F., 2009. Late Quaternary glaciation of the Tianshan, Central Asia, using cosmogenic ^{10}Be surface exposure dating. Quat. Res. 72, 229–233.
Konopelko, D., Biske, G., Seltmann, R., Eklund, O., Belyatsky, B., 2007. Hercynian post-collisional A-type granites of the Kokshaal range, Southern Tien Shan, Kyrgyzstan. Lithos 97, 140–160.
Koppes, M., Gillespie, A., Burke, R., 2008. Late Quaternary glaciation in the Kyrgyz Tien Shan. Quat. Sci. Rev. 27, 846–866.
Kuhle, M., 2004. The High Glacial (Last Ice Age and LGM) ice cover in high and Central Asia. In: Ehlers, J., Gibbard, P. (Eds.), Quaternary Glaciations – Extent and Chronology, Part III. Elsevier, pp. 175–199.
Kuhle, M., 2011. The High Glacial (Last Ice Age and Last Glacial Maximum) ice cover of high and Central Asia, with critical review of some recent OSL and TCN dates. In: Elhers, J., Gibbard, P., Hughes, P.D. (Eds.), Quaternary Glaciations – Extent and Chronology: a Closer Look, Developments in Quaternary Science, second ed. Elsevier, Amsterdam, pp. 943–965.
Lal, D., 1991. Cosmic ray labeling of erosion surfaces: *in situ* nuclide production rates and erosion models. Earth Planet. Sci. Lett. 104, 424–439.
Lal, D., Chen, J., 2005. Cosmic ray labeling of erosion surfaces II: special cases of exposure histories of boulders, soils and beach terraces. Earth Planet. Sci. Lett. 236, 797–813.
Lebedeva, I.M., 1982. Paleoglaciological Assessment for Two Concepts of Late Quarternary Glaciations in Central Asia (in Russian). In: Natural Change in USSR in Late Quarter and Holocene. Moscow State University, Moscow, Russia, pp. 49–53.
Li, J., Li, Z., Zhu, J., Ding, X., Wang, C., Chen, J., 2013. Deriving surface motion of mountain glaciers in the Tuomuer-Khan Tengri Mountain Ranges from PALSAR images. Glob. Planet. Change 101, 61–71.
Li, Y., Liu, G., Kong, P., Harbor, J., Chen, Y., Caffee, M., 2011. Cosmogenic nuclide constraints on glacial chronology in the source area of the Urumqi River, Tian Shan, China. J. Quat. Sci. 26, 297–304.
Li, Y.K., Liu, G.N., Chen, Y.X., Li, Y.N., Harbor, J., Stroeven, A.P., Caffee, M., Zhang, M., Li, C.C., Cui, Z.J., 2014. Timing and extent of Quaternary glaciations in the Tianger Range, eastern Tian Shan, China, investigated using ^{10}Be surface exposure dating. Quat. Sci. Rev. 98, 7–23.
Lifton, N., Bieber, J., Clem, J., Duldig, M., Evenson, P., Humble, J., Pyle, R., 2005. Addressing solar modulation and long-term uncertainties in scaling secondary cosmic rays for *in situ* cosmogenic nuclide applications. Earth Planet. Sci. Lett. 239, 140–161.
Lifton, N., Sato, T., Dunai, T.J., 2014. Scaling *in situ* cosmogenic nuclide production rates using analytical approximations to atmospheric cosmic-ray fluxes. Earth Planet. Sci. Lett. 386, 149–160.
Lifton, N., Smart, D.F., Shea, M.A., 2008. Scaling time-integrated *in situ* cosmogenic nuclide production rates using a continuous geomagnetic model. Earth Planet. Sci. Lett. 268, 190–201.
Lisiecki, L.E., Raymo, M.E., 2005. A Pliocene–Pleistocene stack of 57 globally distributed benthic δ^{18}O records. Paleoceanography 20, 17.
Masarik, J., Wieler, R., 2003. Production rates of cosmogenic nuclides in boulders. Earth Planet. Sci. Lett. 216, 201–208.
Meriaux, A.S., 2004. Rapid slip along the central Altyn Tagh fault: morphochronologic evidence from Cherchen He and Sulamu Tagh. J. Geophys. Res. 109, B06401.
Merzbacher, G., 1905. The Central Tian-Shan Mountains (1902–1903). J. Murray Publishers, London, p. 294.
Mikolaichuk, A., Apayarov, F., Buchroithner, M., Chernavskaja, Z., Skrinnik, L., Ghes, M., Neyevin, A., Charimov, T., 2008. Geological Map of Khan Tengri Massif – Explanatory Note.
Murari, M.K., Owen, L.A., Dortch, J.M., Caffee, M.W., Dietsch, C., Fuchs, M., Haneberg, W.C., Sharma, M.C., Townsend-Small, A., 2014. Timing and climatic drivers for glaciation across monsoon-influenced regions of the Himalayane-Tibetan orogen. Quat. Sci. Rev. 88, 159–182.
Mushketov, I.V., 1915. Turkestan. Geological and Orographical Description Using Data, Collected During Expeditions in 1874–1880. Petrograd.
Narama, C., Kääb, A., Duishonakunov, M., Abdrakhmatov, K., 2010. Spatial variability of recent glacier area changes in the Tien Shan Mountains, Central Asia, using Corona (~1970), Landsat (~2000), and ALOS (~2007) satellite data. Glob. Planet. Change 71, 42–54.
Narama, C., Kondo, R., Tsukamoto, S., Kajiura, T., Duishonakunov, M., Abdrakhmatov, K., 2009. Timing of glacier expansion during the Last Glacial in the inner Tien Shan, Kyrgyz Republic by OSL dating. Quat. Int. 199, 147–156.
Narama, C., Kondo, R., Tsukamoto, S., Kajiura, T., Ormukov, C., Abdrakhmatov, K., 2007. OSL dating of glacial deposits during the Last Glacial in the Terskey-Alatoo Range, Kyrgyz Republic. Quat. Geochronol. 2, 249–254.
Nikonov, A.A., 1982. Paleoglaciological Assessment for Two Concepts of Late Quarternary Glaciations in Central Asia (in Russian). In: Natural Change in USSR in Late Quaternary and Holocene. Moscow State University, Moscow, pp. 54–59.
Nishiizumi, K., 2004. Preparation of ^{26}Al AMS standards. Nucl. Instrum. Methods Phys. Res. Sect. B 223, 388–392.
Nishiizumi, K., Imamura, M., Caffee, M., Southon, J., Finkel, R.C., Mcaninch, J., 2007. Absolute calibration of ^{10}Be AMS standards. Nucl. Instrum. Methods Phys. Res. Sect. B Beam Interact. Mater. Atoms 258, 403–413.
Ochs, M., Ivy-Ochs, S., 1997. The chemical behavior of Be, Al, Fe, Ca and Mg during AMS target preparation from terrestrial silicates modeled with chemical speciation calculations. Nucl. Instrum. Methods Phys. Res. Sect. B 123, 235–240.
Omuralieva, A., Nakajima, J., Hasegawa, A., 2009. Three-dimensional seismic velocity structure of the crust beneath the central Tien Shan, Kyrgyzstan: implications for large-and small-scale mountain building. Tectonophysics 465, 30–44.
Osmonov, A., Bolch, T., Xi, C., Kurban, A., Guo, W., 2013. Glacier characteristics and changes in the Sary-Jaz River Basin (Central Tien Shan, Kyrgyzstan) – 1990–2010. Remote Sens. Lett. 4, 725–734.
Owen, L., Finkel, R.C., Barnard, P., Haizhou, M., Asahi, K., Caffee, M., Derbyshire, E., 2005. Climatic and topographic controls on the style and timing of Late Quaternary glaciation throughout Tibet and the Himalaya defined by Be cosmogenic radionuclide surface exposure dating. Quat. Sci. Rev. 24, 1391–1411.
Owen, L.A., Caffee, M.W., Finkel, R.C., Seong, Y.B., 2008. Quaternary glaciation of the Himalayan-Tibetan orogen. J. Quat. Sci. 23, 513–531.
Owen, L.A., Chen, J., Hedrick, K.A., Caffee, M.W., Robinson, A.C., Schoenbohm, L.M., Yuan, Z., Li, W., Imrecke, D.B., Liu, J., 2012. Quaternary glaciation of the Tashkurgan Valley, Southeast Pamir. Quat. Sci. Rev. 47, 56–72.
Owen, L.A., Dortch, J.M., 2014. Nature and timing of Quaternary glaciation in the Himalayan-Tibetan orogen. Quat. Sci. Rev. 88, 14–54.
Putkonen, J., Swanson, T., 2003. Accuracy of cosmogenic ages for moraines. Quat. Res. 59, 255–261.
Putnam, A.E., Schaefer, J.M., Barrell, D.J.A., Vandergoes, M., Denton, G.H., Kaplan, M.R., Finkel, R.C., Schwartz, R., Goehring, B.M., Kelley, S.E., 2010. *In situ* cosmogenic ^{10}Be production-rate calibration from the Southern Alps, New Zealand. Quat. Geochronol. 5, 392–409.
Ricketts, R.D., Johnson, T.C., Brown, E.T., 2001. The Holocene paleolimnology of Lake Issyk-Kul, Kyrgyzstan: trace element and stable isotope composition of ostracodes. Palaeogeography 176, 207–227.
Rupper, S., Roe, G., 2008. Glacier changes and regional climate: a mass and Energy balance approach*. J. Clim. 21, 5384.
Rupper, S., Roe, G., Gillespie, A., 2009. Spatial patterns of Holocene glacier advance and retreat in Central Asia. Quat. Res. 72, 337–346.
Sciences, R.A.O., 1997. World Atlas of Snow and Ice Resources (in Russian). Russian Academy of Sciences, Moscow.
Severtsov, O.N., 1873. Travels Through Turkestan Region and Research of Tian Shan Mountains (in Russian). Saint Petersburg.
Solomina, O.N., 1999. Mountain Glaciation of Northern Eurasia in the Holocene (in Russian). Scientific World, Moscow.
Sorg, A., Bolch, T., Stoffel, M., Solomina, O., Beniston, M., 2012. Climate change impacts on glaciers and runoff in Tien Shan (Central Asia). Nat. Clim. Change 2, 725–731.
Stone, J., 2000. Air pressure and cosmogenic isotope production. J. Geophys. Res. 105, 23,753–23,759.
Strelow, F., Weinert, C., Eloff, C., 1972. Distribution coefficients and anion exchange behavior of elements in oxalic acid-hydrochloric acid mixtures. Anal. Chem. 44, 2352–2356.
Stroeven, A., Hattestrand, C., Heyman, J., Harbor, J., Li, Y., Zhou, L., Caffee, M., Alexanderson, H., Kleman, J., Ma, H., 2009. Landscape analysis of the Huang He headwaters, NE Tibetan Plateau – Patterns of glacial and fluvial erosion. Geomorphology 103, 212–226.

Stroeven, A.P., Hättestrand, C., Heyman, J., Kleman, J., Morén, B.M., 2013. Glacial geomorphology of the Tian Shan. J. Maps, 1–8.
Tapponnier, P., Molnar, P., 1979. Active faulting and cenozoic tectonics of the Tien Shan, Mongolia, and Baykal regions. J. Geophys. Res. 84, 3425–3459.
Xie, Z., ShangGuan, D., Zhang, S., Ding, Y., Liu, S., 2013. Index for hazard of Glacier Lake outburst flood of Lake Merzbacher by satellite-based monitoring of lake area and ice cover. Glob. Planet. Change 107, 229–237.
Yi, C., Jiao, K., Liu, K., He, Y., Ye, Y., 2002. ESR dating of the sediments of the Last Glaciation at the source area of the Urumqi River, Tian Shan Mountains, China. Quat. Int. 97–98, 141–146.
Yi, C., Liu, K., Cui, Z., Jiao, K., Yao, T., He, Y., 2004. AMS radiocarbon dating of late Quaternary glacial landforms, source of the Urumqi River, Tien Shan—a pilot study of ^{14}C dating on inorganic carbon. Quat. Int. 121, 99–107.
Yin, A., 2010. Cenozoic tectonic evolution of Asia: a preliminary synthesis. Tectonophysics 488, 293–325.
Young, N.E., Schaefer, J.M., Briner, J.P., Goehring, B.M., 2013. A ^{10}Be production-rate calibration for the Arctic. J. Quat. Sci. 28, 515–526.
Zech, R., 2012. A late Pleistocene glacial chronology from the Kitschi-Kurumdu Valley, Tien Shan (Kyrgyzstan), based on ^{10}Be surface exposure dating. Quat. Res. 77, 281–288.
Zech, R., May, J.-H., Kull, C., Ilgner, J., Kubik, P.W., Veit, H., 2008. Timing of the late Quaternary glaciation in the Andes from ~15 to 40° S. J. Quat. Sci. 23, 635–647.
Zech, R., Röhringer, I., Sosin, P., Kabgov, H., Merchel, S., Akhmadaliev, S., Zech, W., 2013. Late Pleistocene glaciations in the Gissar Range, Tajikistan, based on ^{10}Be surface exposure dating. Palaeogeogr. Palaeoclimatol. Palaeoecol. 369, 253–261.
Zhao, J., Zhou, S., He, Y., Ye, Y., Liu, S., 2006. ESR dating of glacial tills and glaciations in the Urumqi River headwaters, Tianshan Mountains, China. Quat. Int. 144, 61–67.
Zhou, S., Jiao, K., Zhao, J., Zhang, S., Cui, J., Xu, L., 2002. Geomorphology of the Urümqi River Valley and the uplift of the Tianshan Mountains in Quaternary. Sci. China Ser. D Earth Sci. 45, 961–968.
Zubovich, A.V., Wang, X.Q., Scherba, Y.G., Schelochkov, G.G., Reilinger, R., Reigber, C., Mosienko, O.I., Molnar, P., Michajljow, W., Makarov, V.I., Li, J., Kuzikov, S.I., Herring, T.A., Hamburger, M.W., Hager, B.H., Dang, Y.-M., Bragin, V.D., Beisenbaev, R.T., 2010. GPS velocity field for the Tien Shan and surrounding regions. Tectonics 29.